Investigation of signal thresholding to reduce the effects of instrument noise of an EMCCD based micro-CT system

Alexander R. Podgorsak[1,3], **Sumukh Bysani Krishnakumar**[1,3], **SV Setlur Nagesh**[3], **Daniel R. Bednarek**[3], **Stephen Rudin**[1,2,3], and **Ciprian N. Ionita**[1,2,3]

[1]Department of Biomedical Engineering, University at Buffalo

[2]Department of Neurosurgery, University at Buffalo

[3]Toshiba Stroke and Vascular Research Center, Buffalo, NY

Abstract

This project investigated the signal thresholding effectiveness at reducing the instrument noise of an electron multiplying charged coupled device (EMCCD) based micro-CT system at low x-ray exposure levels. Scans of a mouse spine and an iodine phantom were taken using an EMCCD detector coupled with a micro-CT system. An iodine filter of 4 mg/cm^2 area density was placed in the beam. The output signal was thresholded using some multiple of the inherent background noise. For each threshold, 100, 200, and 300 frames were summed for each projection to evaluate the effect on the reconstructed image. The projection images from the scans were compared using line profiles and their SNR. Our results indicate that, as the threshold was increased, the line profiles of the projection images showed less statistical variation, but also lower signal levels, so that the SNR of the projection images decreased as the threshold increased. When the line profile of a projection image obtained using a signal threshold is compared with one obtained using energy integrating mode, the profile obtained using thresholding had less variation than that obtained using energy integration, which indicates less instrument noise. The SNR at the edges of the scan object is higher in the thresholded images when compared with the energy integrated projection images. We conclude that thresholding the output signal from an EMCCD detector at low x-ray exposure levels is an effective method to reduce the instrument noise of an EMCCD detector.

Keywords

Signal thresholding; EMCCD; micro-CT; instrument noise

1. INTRODUCTION

The use of charged coupled device (CCD) detectors for the application of medical imaging is well established in professional practice. There is much variability in what sort of data the CCD detector can obtain, depending on what sort of system is set up. Applications such as fluoroscopy, mammography, and standard radiography are all possible using a CCD detector[9]. In this day, it is the responsibility of the medical imager to reduce the radiation dose that the image object will get. However, this reduction in dose must not negatively impact the quality of the images obtained, or else it is needless dose to the patient[13].

Currently, at low signal levels that would be desirable for the reduction of dose to the patient, standard CCD detectors are limited by the readout noise of the output converter to a voltage[4].

In an attempt to rectify this problem with the standard CCD detector, two types of variations were developed, the intensified CCD (ICCD) and the electron multiplying CCD (EMCCD). The ICCD detector is a standard cooled CCD camera which is fiber-optically coupled to an image intensifier[6]. The ICCD is not the focus of this paper, and is already well described in the literature[7, 8].

The EMCCD detector was the other modification to the standard CCD camera. The exact operation of the EMCCD camera is well described in Jerram *et al.*[12] and Mackay *et al.*[16]. A short description will be included here however. Additionally, a schematic diagram of the electron multiplying process and the extra multiplication register can be found in Figure 1 below. The basic principle of how the charge is multiplied is analogous to that of an avalanche photodiode[18]. The EMCCD camera works by multiplying the charge before the conversion into a voltage. The registers used are conventional from the standard CCD. At the end of the process, before the charge-to-voltage converter, there is an extra register included, called a multiplication register. The number of electrons passing through each multiplication element is increased using increased potential[17]. Following the multiplication register, the charge is converted to a voltage. In this way, the gains that are yielded in the charge domain do not lead to the limiting effects from the readout noise that is seen in the standard CCD[10]. The EMCCD detector is capable of detecting a very weak signal, and amplifying it several hundred times to output a signal with a gain that can be three orders of magnitude larger than the original signal. In this way, the negative effect of the readout noise due to the conversion to a voltage is minimized[14].

For the majority of applications, the EMCCD detector works well. The electron multiplying process causes the error due to readout noise to be at the sub-electron level[15]. Many research groups have successfully used the electron multiplying characteristics of the EMCCD to develop EMCCD based systems for fluoroscopy[19], radiography, photon-counting gamma cameras[1], and even combined SPECT/CT[20].

Each of the electron transfers will have some noise attached to it however[12]. Over the course of the entire charge multiplication, this noise can add up and will reduce the quality of the images that are obtained using the EMCCD detector. It is this instrument noise that we attempted to minimize.

We have developed a micro-CT system dedicated to the imaging of small animals and objects. Exact details of the system can be found in the paper by Ionita *et al.*[22], and a schematic of the entire system can be found in Figure 2 below. For this application, we are focusing on micro-CT scan of small samples at low energies where there are x-ray tube restrictions on the mA. This causes operation of the detector at exposures close to the instrumentation noise equivalent exposure. The strategy that we chose to solve this problem was to use signal thresholding as a percentage of the dark field variation at each pixel. Such a strategy was previously investigated by Basden *et al.*[2]. In this way, the instrument noise

that would typically reduce the quality of the image obtained from an EMCCD detector is minimized.

Two thresholds were used and their effects on the final output image were investigated. Each time an image is being acquired, the matrix which is the digital representation of the image is passed through the two thresholds. First, a "floor" threshold was used to remove the low intensity instrument noise which reduces the quality of the image. If an image element is below the threshold, it is set to zero and its impact on the final image is removed. An assumption is made that each photon should have equal weight on the final image. A second threshold, called a "count" threshold, is used because of this assumption. If an image element passes through the first threshold, its value is replaced with a lower, constant value.

2. METHODOLOGY

In order to filter the x-ray beam, an iodine filter was placed in the x-ray beam. Padežnik *et al.* had determined that the k-edge of iodine was around 33 keV[3]. This filter accomplishes two things. First, it reduces the x-ray exposure the scan object will receive. Second, the iodine filter will cause the beam to be more monochromatic than an unfiltered beam. This would prevent the streaking artifacts that are sometimes seen in reconstructions of CT images. Using an ionization chamber, the exposure at the scan object was determined to be 160 μR/frame using x-ray tube parameters that output 0.5 mAs and 40 kVp, and an EMCCD detector exposure time of 100 ms/frame.

The next step was to determine the instrument noise of the EMCCD detector. To this end, 60 images were taken without any x-rays at a reference gain level. These images were analyzed pixel by pixel to see how the mean and standard deviation vary over the 60 images taken at the level of detector gain selected. The resulting mean of each pixel over the 60 images, shown in Figure 3-left, can be thought of as the dark-field for the EMCCD detector, and the resulting variance of each pixel over the 100 images, shown in Figure 3-right, can be thought of as the instrument noise. This is what is used for the floor threshold which determines if an image element will be counted in the final image or not.

Next, we scanned a mouse spine using x-ray tube parameters of 40 kVp and 30 W using the iodine filter in the beam. As was explored by O'Malley *et al.*, a number of frame additions would be used for each projection[5]. Three output frame numbers would be considered; one at 100 frame additions, a second at 200, and a third at 300. The output signal from the EMCCD detector is processed using the LabVIEW programming language. The signal processing steps are as follows; the raw output signal, obtained using a 100 ms exposure time on the EMCCD detector is dark-field corrected by subtracting the left image in Figure 3 which contains the mean of values for each pixel in the 100 dark frames. The dark-field corrected image is then compared using the floor threshold that was determined previously. Each frame was compared with 0.5 or 1.0 multiplied by the variance of each of the pixel values over the 100 dark images (right image Figure 3). If the pixel being thresholded lies below the multiple of variance image, it is set to zero. After this threshold comparison is carried out, the frames are passed through one final threshold, the so-called "count" threshold. If a value of a pixel is within a specified range, in this case between 10 and 1000,

the value is replaced with 1. In this way, each photon event only has an effect on the final image due to its occurring, not due to its actual magnitude. The image pixel values are then added until the specific frame numbers that are being considered; 100, 200, and 300 frame additions. After the specific frame additions are met, the resulting image is flat field corrected. There is a specific flat field for each amount of frame additions. An example of an individual un-added frame (Figure 4 left) as well as a projection image (Figure 4 right) that is yielded from the frame additions can be seen below. It is at these frame addition numbers that the images will be flat field corrected, then output to a raw image file which can be analyzed. Energy integration mode was also used for a comparison. The iodine filter was removed for the scans using energy integration mode. The tube parameters were kept constant, yet the EMCCD exposure time was increased to 500 ms/frame.

Following the scans of the mouse spine, a more consistent scan object was desired. A 3D-printed phantom with six liquid iodine contrast agent inserts was developed in-house for this purpose. The 3D-printed iodine phantom would be scanned using x-ray parameters of 40 kVp and 40 W again using the iodine filter in the beam. Due to the fact that the tube parameters were changed, and the EMCCD detector exposure time was reduced to 5 ms/frame, the exposure at the scan object was lowered to 8.2 μR/frame. Only additions of 300 frames would be considered during the iodine phantom scans, as the best results in terms of SNR stem from more frame additions. Different from the spine scans, however, was the threshold multiple. Recall that during the spine scans, the two floor threshold multiples used were 0.5 and 1.0. During the iodine phantom scans, a threshold multiple of 0.1 from the variance image would be used. During the scans of the iodine phantom, only one gain level was used; the one which yielded the superior SNRs from the scans of the mouse spine. A different EMCCD detector was used for the iodine phantom scans. This one has a larger field of view when compared with the original EMCCD detector used for the mouse spine scans. This allowed for magnification to be used when scanning the iodine phantom, so the phantom could be smaller than the size of the mouse spine.

Additionally, a scan was performed to ascertain what effect the count threshold actually had on the final output image. A scan was performed disabling the count threshold, and was compared with a scan that had a count threshold which replaced any pixel value between 5 and 50 with a value of 2. All other scan parameters were kept constant from the previously described iodine phantom scan.

For the analysis and comparison of the images, quantitative metrics were used. Line profiles over a consistent location on each of the projection images were taken using ImageJ and analyzed for signal amplitude at the beginning and ending edge of the mouse spine and iodine phantom, as well as the contrast between the background and the spine. SNR calculations for the mouse spine were done using projection images, taking regions of interest (ROI's) at both the center of the vertebral body, as well at the edge. SNR calculations for the iodine phantom were done using reconstructed images, taking ROI's inside of the iodine inserts. Reconstruction was done using a standard FDK algorithm which employs a self-correction of the rotational axis. More detail regarding this self-calibration can be found in the paper by Patel et al.[23]. We suspected that the projection images obtained using signal thresholding will be superior to images obtained using energy integration at the

edges of the mouse spine and the iodine phantom. Additionally, we expected the count thresholded projection images to have a higher SNR than those which were obtained using a disabled count threshold.

3. RESULTS

3.1 Mouse Spine Scan Results

The line profile taken using a projection image of the mouse spine and two different floor threshold multiples (0.5 and 1.0) can be found in Figure 5. Included in Figure 5 is an example of a projection of the mouse spine taken using a floor threshold multiple of 0.5 and an addition of 300 frames for each projection angle.

Projection images of the mouse spine obtained using 100, 200, and 300 frame additions were reconstructed using the modified FDK algorithm described earlier. The reconstructed slices of the spine can be found in Figure 6 below. For the projection images used, a constant floor threshold multiple of 0.5 was used.

A comparison between a projection image taken using signal thresholding and a projection taken using energy integrating mode can be found in Figure 7 below. The signal thresholding was performed using a floor threshold multiple of 0.5 and 300 frames per projection. Included in Figure 7 are two ROIs that are used in the SNR calculations in Table 1. The ROI seen in Figure 7a is the one used for the center of vertebra SNR calculations. The ROI seen in Figure 7b is the one used for the edge of vertebra SNR calculation.

All the SNR calculations done using projection images of the mouse spine can be found in Table 1. These calculations were carried out taking signal from two different locations on the mouse spine, either in the center of the vertebra or at the edge. Two different levels of EMCCD gain were used as well, to ascertain the impact of using a lower level on the resulting SNR.

3.2 Iodine Phantom Scan Results

In Figure 8 below, examples of projection images of the iodine phantom can be found. The three projection images were obtained using two different thresholding schemes (Figure 8a and 8b), and one standard energy integration mode (Figure 8c). The projection in Figure 8a was obtained by disabling the second "count" threshold. The projection in Figure 8b was obtained by enabling the "count" threshold. In the two cases where signal thresholding was employed, 300 frame additions per projection were used, and a floor threshold multiple of 0.1 was used. The level of EMCCD gain used was the same reference level of gain from the mouse spine scans.

Next, reconstructed volumes of the iodine phantom were computed using the three sets of projection data obtained using the two thresholding strategies and energy integration mode. The reconstruction was again carried out using the modified FDK reconstruction algorithm described earlier. The reconstructed images of the projection images obtained using the three different strategies can be found in Figure 9.

SNRs were then taken using the reconstructed slices of the iodine phantom using projections obtained through the use of three different image acquisition strategies; two signal thresholding schemes and energy integration mode. The results of this can be found in Table 2. Two different ROIs were used to take the background portion of the SNR calculation. The ROI locations can be found in Figure 9a and Figure 9b.

4. DISCUSSION

In this work, we have reported on the effectiveness of using a thresholding scheme to reduce the impact of electronic noise which results from the electron multiplying process of an EMCCD detector. There are several parameters which will affect the threshold used. The effect of these various parameters will be discussed in this section.

The multiple of the floor threshold used has a large impact on the final output image. If the threshold multiple is too high, very little of the signal will get through, and quantum mottle will affect the image. If the threshold multiple is too low, the electronic noise will affect the image. In Figure 5, line profiles using projection images obtained using two threshold multiples were shown. The 0.5 threshold multiple profile had greater variation than the 1.0 threshold multiple profile. This indicates that instrument noise had a greater impact on the 0.5 threshold projection image. Yet, signal amplitude was lower for the 1.0 threshold multiple profile (especially at the edges of the objects in the field of view). This indicates that part of the actual signal is being cut out in the 1.0 threshold multiple projection image. Due to this, more trabecular detail can be gathered from the 0.5 threshold multiple as opposed to the 1.0 threshold multiple.

When the reconstructed slices of the mouse spine computed using the three different frame amounts per projection are compared qualitatively, as shown in Figure 6, there are differences between the three. The background of the slice obtained using 100 frame additions has less uniformity, and the edges of vertebral body are less sharp. It is difficult to see the trabecular detail of the spine. There is less of a difference between the 200 and 300 frame additions per projection. The edges are marginally sharper in the 300 frame additions per projections. Yet, 200 frames seem to be enough when the reconstructed slices are considered. The trabecular detail can be discerned using 200 frames per projections.

A comparison between a projection obtained using signal thresholding and a projection obtained using energy integration mode is shown in Figure 7. The background of the projections is less uniform in the signal thresholding projections when compared with the energy integrating mode. The edge of the spine, however, seems to be sharper in the signal thresholding projection than in the energy integrating projection.

The list of SNRs that are found in Table 1 yield a positive result towards the use of signal thresholding. At optimal conditions, meaning 300 frame additions, a floor threshold multiple of 0.5, and an ROI taken at the edge of the mouse spine, signal thresholding can yield a better SNR than that of energy integrating mode. At the reference gain level of EMCCD, no other thresholding parameters were able to match what energy integrating mode could do. When a lower gain level was selected, and the SNR is compared with those from the higher

gain level, the SNR is lower. This is an interesting result. A lower EMCCD gain level would lead to less impact from the uncertainty in the electron multiplication process described in the introduction. However, a lower gain level would lead to more impact from the uncertainty of the output converter. This is the uncertainty which is addressed by using the EMCCD in the first place. In this case, the increased uncertainty from the output converter drops the SNR more than the decreased uncertainty from the electron multiplying process can raise it.

The comparison between two different types of signal thresholding in Figure 8 yielded a surprising result. There was no real advantage gained by enabling the count threshold. This conclusion was reached using the qualitative result from a comparison of the projections of the iodine phantom, a comparison of the reconstructed slices of the iodine phantom, and backed up with the SNR calculations found in Table 2 which were taken using the reconstructed slices. The two thresholding schemes yielded similar results in every facet. The projections, reconstructed slices, and SNR values were all similar. When the projections obtained using the two thresholding schemes were compared with the projections obtained using energy integrating mode, results similar to the mouse spine scan were yielded. The background was less uniform for the signal thresholded projections, yet the edges were sharper. This is backed up with the SNR calculations found in Table 2 as well.

The SNRs found in Table 2 tell a similar story to those found in Table 1. Signal thresholding, at optimal conditions of 300 frame additions per projection angle, a high level of EMCCD gain, and a floor threshold multiple of at or less than 0.5, is capable of obtaining superior SNR when compared with energy integrating mode. This result was achievable using two different EMCCD detectors, imaging two different objects of different size and material.

The one worrying result from using signal thresholding is yielded after the reconstructed slices of the iodine phantom were obtained. The large degrading qualitative factor of the reconstructions of projections obtained using the thresholding schemes is the presence of heavy ring artifacts in the central region of the slices. These rings are replaced in the energy integrating reconstruction by the presence of streaks. The streaks seem to be prevented in the thresholded reconstructions by the use of the iodine filter. It does appear, however, that the ring artifacts that are present in Figure 9a and Figure 9b are independent of the thresholding scheme.

5. CONCLUSION

We have described and reported on the effectiveness of signal thresholding for the reduction of electronic noise caused by the amplification process of an EMCCD detector. We have shown that at low x-ray exposure levels, where the assumption that only a few photons are detected by each pixel is acceptable, the use of a threshold of some multiple from the standard deviation of the dark field is effective at reducing the instrument noise. Even at 100 frame additions, trabecular detail of the mouse spine can be seen in a reconstructed image. At higher numbers of frame additions, the edges of the spine become sharper, and even more detail can be seen. At the edge of the mouse spine, signal thresholding can yield a higher SNR than energy integrating mode. Similar results were ontained when the iodine phantom

was scanned. The SNR of reconstructed slices of the iodine phantom were higher when projections obtained through the use of signal thresholding were used when compared with projections obtained using energy integrating mode. It was determined, however, that the second threshold, the "count" threshold, does not appreciably improve the image in terms of SNR of the iodine phantom. This strategy of signal output thresholding is most effective at the low x-ray exposure levels which are obtained through the use of the iodine filter.

Acknowledgments

References

1. de Vree GA, Westra AH, Moody I, van der Have F, Ligtvoet KM, Beekman FJ. Photon-Counting Gamma Camera Based on an Electron-Multiplying CCD. IEEE Trans Nucl Sci. 2005; 52(3):580–588.

2. Basden AG, Haniff CA, Mackay CD. Photon counting strategies with low-light-level CCDs. Mon Not R Astron Soc. 2003; 345:985–991.

3. Padeznik Gomilsek J, Arcon I, de Panfilis S, Kodre A. X-ray absorption coefficient of iodine in the k edge region. J Phys B: At Mol Opt Phys. 2008; 41:1–5.

4. Dussault D, Hoess P. Noise performance comparison of ICCD with CCD and EMCCD cameras. Proc SPIE. 2004; 5563:195–204.

5. O'Malley MJ, O'Mongain E. Charge-coupled devices: frame adding as an alternative to long integration times and cooling. Opt Eng. 1992; 31(3):522–526.

6. Denvir DJ, Conroy E. Electron multiplying CCD technology: The new ICCD. Proc SPIE. 2003; 4796:164–174.

7. Moran SE, Ulich BL, Elkins WP, Strittmatter RL, DeWeert MJ. Intensified CCD (ICCD) dynamic range and noise performance. Proc SPIE. 1997; 3173:430–457.

8. Denvir DJ, Coates CG. Electron multiplying CCD Technology: Application to ultrasensitive detection of biomolecules. Proc SPIE. 2002; 4626:502–512.

9. Janesick, JR. Scientific Charged-Coupled Devices. SPIE Press; Bellingham, Washington: 2001.

10. Hynecek J, Nishiwaki T. Excess noise and other important characteristics of low light level imaging using charge multiplying CCDs. IEEE Trans Electron Devices. 2003; 50(1):239–245.

11. Hynecek J. Impactron-A new solid state image intensifier. IEEE Trans Electron Devices. 2001; 48:2238–2241.

12. Jerram P, Pool P, Bell R, Burt D, Bowring S, Spencer S, Hazelwood M, Moody I, Catlett N, Heyes P. The LLLCCD: Low light imaging without the need for an intensifier. Proc SPIE. 2001; 4306:178–186.

13. Harris EJ, Royle GJ, Speller RD, Spencer S, Suske W. Evaluation of a novel CCD camera for dose reduction in digitial radiography. Nuclear Science Symposium Conference Record. 2000; 3:53–58.

14. Hynecek J. CCM-A new low-noise charge carrier multiplier suitable for detection of charge in small pixel CCD image sensors. IEEE Trans Electron Devices. 1992; 39(8):1972–1975.

15. Beekman F, deVree GA. Photon-counting versus an integrating CCD-based gamma camera: important consequences for spatial resolution. Phys Med Biol. 2005; 50:109–119.

16. Mackay CD, Tubbs RN, Bell R, Burt D, Jerram P, Moody I. Sub-electron read noise at MHz pixel rates. Proc SPIE. 2001; 4306:289–298.

17. Robbins MS, Hadwen BJ. The noise performance of electron multiplying charge coupled devices. IEEE Trans Electron Devices. 2003; 50(5):1227–1232.

18. Hollenhorst JN. A theory of multiplicative noise. IEEE Trans Electron Device. 1990; 37(3):781–788.

19. Kuhls AT, Yadava G, Patel V, Bednarek D, Rudin S. Progress in electron multiplying CCD (EMCCD) based high-resolution, high sensitivity x-ray detector for fluoroscopy and radiography. Proc SPIE. 2007; 6510:1–15.

20. Nagarkar VV, Singh B, Shestakova I, Gaysinkiy V. Design and performance of an EMCCD based detector for combined SPECT/CT imaging. IEEE Nucl Sci Symp Conf Record. 2005; 4:2179–2182.

21. deVree GA, Westra AH, Moody I, van der Have F, Ligtvoet KM, Beekman FJ. Electronics for a photon-counting gamma camera based on an electron-multiplying CCD. IEEE Nucl Sci Symp Conf Recond. 2004; 7:4159–4163.

22. Ionita CN, Hoffmann KR, Bednarek DR, Chityala R, Rudin S. Cone-beam micro-CT system based on LabVIEW software. J Digit Imaging. 2008; 21(3):296–305. [PubMed: 17333411]

23. Patel V, Chityala RN, Hoffman KR, Ionita CN, Bednarek DR, Rudin S. Self-calibration of a cone-beam micro-CT system. Med Phys. 2009; 36(1):48–58. [PubMed: 19235373]
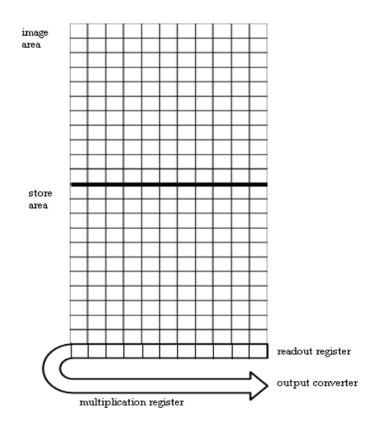
Figure 1.
Diagram of an EMCCD which shows the extra multiplication register before the output converter. The result of the electron multiplying process is a reduction in the effects of readout noise when compared with a standard CCD detector.
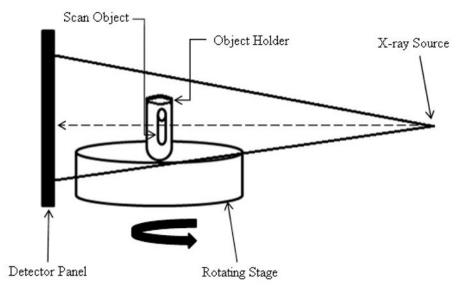
Figure 2.
Diagram of the custom micro-CBCT system used in this project. Shown is the scan object on a rotating stage. The detector and x-ray source are stationary in this system.
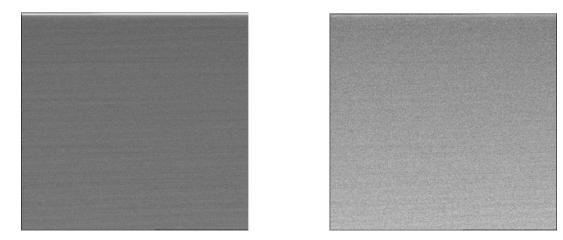
Figure 3.
Images show the mean (left) and variance (right) of the pixel values over 60 frames at a reference gain level. The mean image is used as a dark field; the variance image is used as a signal threshold. These results are in agreement with de Vree *et al.*[21]
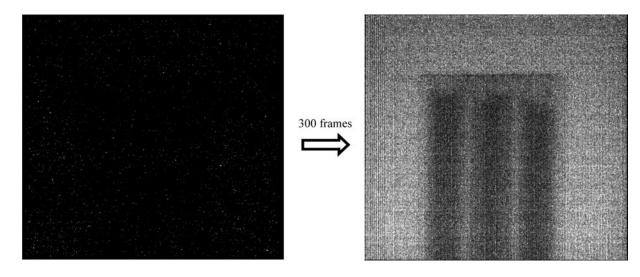
Figure 4.
Image of a single frame after the signal thresholding scheme (left), obtained using an
EMCCD exposure time of 5ms. This frame is added with 100, 200, and 300 others to yield
an image similar to that on the right, which is an uncorrected projection image of the iodine
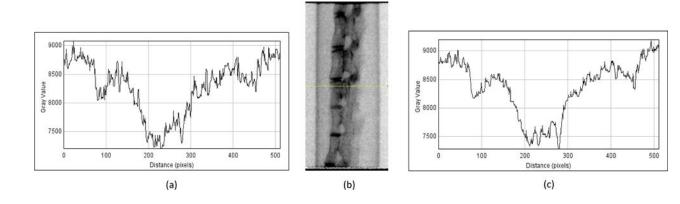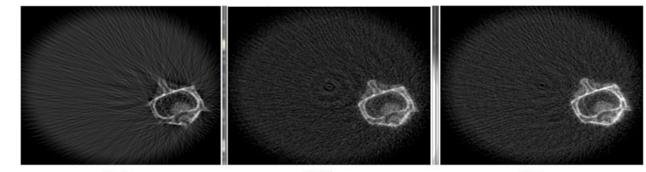phantom prior to a flat field correction being applied on it.

Figure 5.
Line profiles showing less variability as the threshold is increased. (b) is a projection obtained using a floor threshold multiple of 0.5 and adding 300 frames, showing the location (yellow line) where the line profiles were taken for all projections taken during the mouse spine scan. (a) is a line profile taken using a projection obtained with a floor threshold multiple of 0.5 and adding 100 frames. (c) is a line profile taken using a projection obtained with a floor threshold multiple of 1.0 and adding 100 frames.

100 frames 200 frames 300 frames

Figure 6.
Three reconstructed images of the mouse spine using projections obtained by adding 100, 200, and 300 frames per projection. Reconstruction was done using a modified FDK algorithm.
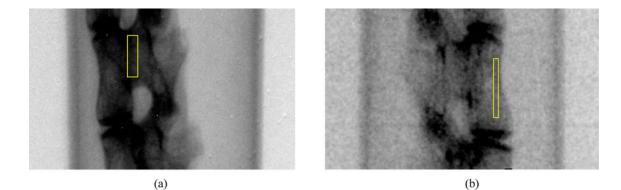
(a)   (b)

Figure 7.
(a) is a projection obtained using energy integration mode during a scan of the mouse spine. It shows where the ROI (yellow rectangle) was taken for the center of vertebra SNR calculations. (b) is a projection obtained using a floor threshold of 0.5 adding 300 frames during the scan of the mouse spine. It shows where the ROI (yellow rectangle) was taken for the edge of vertebra SNR calculations.
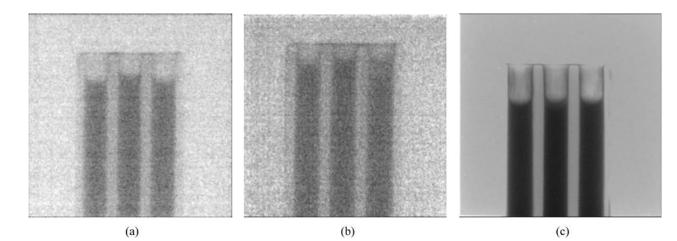
Figure 8.
(a) is a projection image of the iodine phantom without the count threshold. (b) is a projection image of the iodine phantom with the count threshold. (c) is a projection image of the iodine phantom obtained using energy integrating mode.
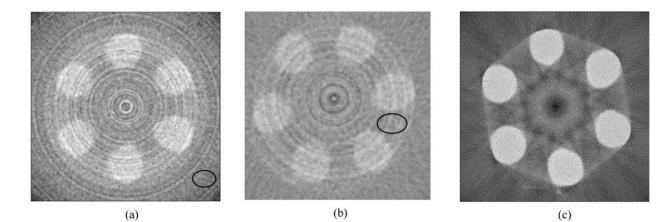
Figure 9.
(a) is a reconstructed image of the iodine phantom from projections seen in Figure 6a without the count threshold. ROI shown is the background used during the "background air" SNR calculation seen in Table 2. (b) is a reconstructed image of the iodine phantom from projections seen in Figure 6b with the count threshold. ROI shown is the background used during the "background phantom" SNR calculation also seen in Table 2. (c) is a reconstructed image of the iodine phantom from projections seen in Figure 6c using energy integrating mode.

Table 1

List of SNRs of projection images obtained using different strategies during scans of the mouse spine. The data suggests that 200 frame additions is not sufficient to better energy integrating mode in terms of SNR at the edge of the vertebra. All 300 frames are needed.

Gain	Edge of Vertebra	SNR	Center of Vertebra	SNR
Reference	**0.5σ 100 frames**	10.9	**0.5σ 100 frames**	9.83
	0.5σ 200 frames	13.9	**0.5σ 200 frames**	11.4
	0.5σ 300 frames	15.4	**0.5σ 300 frames**	14.3
	1.0σ 100 frames	10.5	**1.0σ 100 frames**	8.42
	1.0σ 200 frames	12.0	**1.0σ 200 frames**	10.2
	1.0σ 300 frames	13.1	**1.0σ 300 frames**	10.8
	Energy Integration	14.5	**Energy Integration**	14.8
2.5 times lower	**0.5σ 100 frames**	5.00	**0.5σ 100 frames**	3.88
	0.5σ 200 frames	6.21	**0.5σ 200 frames**	4.82
	0.5σ 300 frames	7.39	**0.5σ 300 frames**	5.85

Table 2

List of SNRs of reconstructed slices of the iodine phantom obtained using two thresholding strategies and energy integration. ROIs considered were from two locations shown in Figure 7. Reconstruction performed using a standard FDK algorithm.

Background Air	SNR	Background Phantom	SNR
Count threshold disabled	7.2	Count threshold disabled	5.2
Count threshold enabled	7.1	Count threshold enabled	5.9
Energy Integration	5.3	Energy Integration	3.6